

# Octupole deformation in the ground states of even-even $Z \sim 96$ , $N \sim 196$ actinides and superheavy nuclei

S. E. Agbemava and A. V. Afanasjev

*Department of Physics and Astronomy, Mississippi State University, Mississippi 39762, USA*

(Received 4 May 2017; revised manuscript received 27 June 2017; published 3 August 2017)

A systematic search for axial octupole deformation in the actinides and superheavy nuclei with proton numbers  $Z = 88$ –126 and neutron numbers from the two-proton drip line up to  $N = 210$  was performed in covariant density functional theory (DFT) using four state-of-the-art covariant energy density functionals representing different model classes. The nuclei in the  $Z \sim 96$ ,  $N \sim 196$  region of octupole deformation were investigated in detail and the systematic uncertainties in the description of their observables were quantified. A similar region of octupole deformation exists also in Skyrme DFT and microscopic+macroscopic approaches but it is centered at somewhat different particle numbers. Theoretical uncertainties in the predictions of the regions of octupole deformation increase on going to superheavy nuclei with  $Z \sim 120$ ,  $N \sim 190$ . There are no octupole deformed nuclei for  $Z = 112$ –126 in covariant DFT calculations. This agrees with Skyrme DFT calculations, but disagrees with Gogny DFT and microscopic+macroscopic calculations which predict an extended  $Z \sim 120$ ,  $N \sim 190$  region of octupole deformation.

DOI: [10.1103/PhysRevC.96.024301](https://doi.org/10.1103/PhysRevC.96.024301)

## I. INTRODUCTION

Reflection asymmetric (or octupole deformed) shapes represent an interesting example of symmetry breaking of the nuclear mean field [1]. They are present in the ground and rotating states of the lanthanides with  $Z \sim 58$ ,  $N \sim 90$  and light actinides with  $Z \sim 90$ ,  $N \sim 136$  (see Refs. [1–4] and references quoted therein). These shapes also affect the outer fission barriers in actinides and superheavy nuclei [5–7] and cluster radioactivity [8]. The first significant wave of studies of octupole deformed shapes took place in the 1980s and the first half of the 1990s (see the review in Ref. [1]). The interest in studying such shapes has significantly increased during the present decade (see references on theoretical and experimental works quoted in Ref. [4]).

Different theoretical frameworks have been used for the study of octupole deformed shapes (see Refs. [1,4,6] and references quoted therein). Here we employ the covariant density functional theory (CDFT) [9]. Its previous applications to the investigation of such shapes have been overviewed and compared with the results of nonrelativistic studies in Ref. [4]. Built on Lorentz covariance and the Dirac equation, CDFT provides a natural incorporation of spin degrees of freedom [10,11] and a good parameter-free description of spin-orbit splittings [11–13], which have an essential influence on the underlying shell structure. In addition, in CDFT the time-odd components of the mean fields are given by the spatial components of the Lorentz vectors. Therefore, because of Lorentz invariance, these fields are coupled with the same constants as the timelike components [14], which are fitted to ground state properties of finite nuclei (which are affected only by time-even mean fields) and nuclear matter properties.

Starting from the pioneering work of Ref. [15], the CDFT has been extensively used in the study of reflection asymmetric shapes, especially during the last decade. Most of these applications have been focused on reflection symmetric shapes with axial symmetry; they were reviewed in Ref. [4]. Let us

mention some of these studies performed in the actinides. At the mean field level, the ground state properties of the actinides were studied in Refs. [4,15–19]. Some axial octupole deformed nuclei have been studied also in the beyond-mean-field approaches based on CDFT. For example, simultaneous quadrupole and octupole shape phase transitions in the Th isotopes were studied in Ref. [17] employing microscopic collective Hamiltonian. Using the interacting boson model Hamiltonian—with parameters determined by mapping the microscopic potential energy surfaces, obtained in relativistic Hartree-Bogoliubov calculations, to the expectation value of the Hamiltonian in the boson condensate—the microscopic analysis of the octupole phase transition was performed in Refs. [18,19]. Generator coordinate method studies taking into account dynamical correlations and quadrupole-octupole shape fluctuations were undertaken in  $^{224}\text{Ra}$  employing the PC-PK1 functional in Ref. [20]. They revealed rotation-induced octupole shape stabilization.

Nonaxial-octupole  $Y_{32}$  correlations in the  $N = 150$  isotones and tetrahedral shapes in neutron-rich Zr isotopes were studied in Refs. [21,22] employing multidimensional constrained CDFT. Although the energy gain due to  $\beta_{32}$  distortion exceeds 300 keV in  $^{248}\text{Cf}$  and  $^{250}\text{Fm}$  in model calculations, it is not likely that static deformation of this type is present in nature in these two nuclei. This is because their rotational features are well described in the cranked relativistic Hartree-Bogoliubov framework with no octupole deformation [23,24]. Despite theoretical predictions and substantial experimental efforts, a clear experimental signal of tetrahedral shapes is still absent (see the discussion in the introduction of Ref. [22]). In addition, symmetry unrestricted multidimensional constrained CDFT calculations are extremely time-consuming. For these reasons, only reflection symmetric shapes with axial symmetry are considered in the present paper.

The most comprehensive study of octupole deformed shapes at the mean field level within the CDFT framework was performed in Ref. [4]. In that paper the global search for



such shapes was carried out in all  $Z \leq 106$  even-even nuclei located between two-proton and two-neutron drip lines with two covariant energy density functionals (CEDFs) NL3\* and DD-PC1. As a result, a new region of octupole deformation, centered around  $Z \sim 98$ ,  $N \sim 196$  was found in the CDFT framework for the first time. Based on the results obtained with these two functionals it was concluded that in terms of its size in the  $(Z, N)$  plane and the impact of octupole deformation on binding energies, this region is similar to the best known region of octupole deformed nuclei centered at  $Z \sim 90$ ,  $N \sim 136$ . In addition, the systematic uncertainties in the description of the ground states of octupole deformed nuclei in the  $Z \sim 58$ ,  $N \sim 90$  lanthanides and  $Z \sim 90$ ,  $N \sim 136$  actinides were defined for the first time in the CDFT framework using five state-of-the-art CEDFs representing different classes of the CDFT models.

However, a number of questions still remain unresolved in Ref. [4]. The search for the answers to these questions is the main goal of this paper. First, there are the indications that octupole deformation can be present in the ground states of superheavy elements (SHE) with  $Z \geq 108$ ,  $N \sim 190$ . They come from the results of the calculations within the microscopic+macroscopic (mic+mac) approach [25] and nonrelativistic Hartree-Fock-Bogoliubov (HFB) method based on the finite range Gogny D1S force [26]. To our knowledge no search of octupole deformation in the ground states of superheavy  $Z \geq 108$  nuclei has been performed within the CDFT framework so far. To fill this gap in our knowledge we will perform such a search in the region of proton numbers  $108 \leq Z \leq 126$  and in the region of neutron numbers from the two-proton drip line up to neutron number  $N = 210$ . This region almost coincides with the region used in a recent reexamination of the properties of SHE in the CDFT framework in Ref. [27].

Second, we will establish systematic theoretical uncertainties in the predictions of the properties of the octupole deformed nuclei in the  $Z \sim 98$ ,  $N \sim 196$  mass region and in superheavy nuclei. This is important since these nuclei will not be accessible with future facilities such as the Facility for Rare Isotope Beams (FRIB). However, the accounting of octupole deformation in the ground states of these nuclei is essential for the modeling of fission recycling in neutron star mergers [28,29] since the gain in binding energy of the ground states due to octupole deformation will increase the fission barrier heights as compared with the case when octupole deformation is neglected.

To achieve these goals we use the four most up-to-date covariant energy density functionals of different types: with a nonlinear meson coupling (NL3\* [30]), with density-dependent meson couplings (DD-ME2 [31]), and with density-dependent zero-range interactions (DD-PC1 [32] and PC-PK1 [33]). They represent different classes of CDFT models (see the discussion in Ref. [34]). The functional DD-ME $\delta$  used in our previous studies of the global performance of CDFT [4,27,34–37] is not employed here since it fails to reproduce octupole deformation in light actinides [4] and inner fission barriers in superheavy nuclei [37].

The paper is organized as follows. Section II describes the details of the solutions of the relativistic Hartree-Bogoliubov

equations. Section III is devoted to the discussion of the ground state properties of octupole deformed nuclei and their dependence on the covariant energy density functional. The evolution of potential energy surfaces with proton and neutron numbers is discussed in Sec. IV. The assessment of systematic theoretical uncertainties in the predictions of ground state properties of octupole deformed nuclei and the comparison with other model predictions are performed in Sec. V. Finally, Sec. VII summarizes the results of our work.

## II. THE DETAILS OF THE THEORETICAL CALCULATIONS

The calculations were performed in the Relativistic-Hartree-Bogoliubov (RHB) approach using the parallel computer code RHB-OCT developed in Ref. [4]. Note that only axial reflection asymmetric shapes are considered in this code.

The calculations in the RHB-OCT code perform the variation of the function

$$E_{RHB} + \sum_{\lambda=2,3} C_{\lambda 0} (\langle \hat{Q}_{\lambda 0} \rangle - q_{\lambda 0})^2 \quad (1)$$

employing the method of quadratic constraints. Here  $E_{RHB}$  is the total energy (see Ref. [34] for more details of its definition) and  $\langle \hat{Q}_{\lambda 0} \rangle$  denote the expectation values of the quadrupole ( $\hat{Q}_{20}$ ) and octupole ( $\hat{Q}_{30}$ ) moments, which are defined as

$$\hat{Q}_{20} = 2z^2 - x^2 - y^2, \quad (2)$$

$$\hat{Q}_{30} = z(2z^2 - 3x^2 - 3y^2). \quad (3)$$

$C_{20}$  and  $C_{30}$  in Eq. (1) are corresponding stiffness constants [38] and  $q_{20}$  and  $q_{30}$  are constrained values of the quadrupole and octupole moments. In order to provide the convergence to the exact value of the desired multipole moment, we use the method suggested in Ref. [39]. Here the quantity  $q_{\lambda 0}$  is replaced by the parameter  $q_{\lambda 0}^{\text{eff}}$ , which is automatically modified during the iteration in such a way that we obtain  $\langle \hat{Q}_{\lambda 0} \rangle = q_{\lambda 0}$  for the converged solution. This method works well in our constrained calculations. We also fix the (average) center of mass of the nucleus at the origin with the constraint

$$\langle \hat{Q}_{10} \rangle = 0 \quad (4)$$

on the center-of-mass operator  $\hat{Q}_{10}$  in order to avoid a spurious motion of the center of mass.

The charge quadrupole and octupole moments are defined as

$$Q_{20} = \int d^3r \rho(\mathbf{r}) (2z^2 - r_{\perp}^2), \quad (5)$$

$$Q_{30} = \int d^3r \rho(\mathbf{r}) z(2z^2 - 3r_{\perp}^2) \quad (6)$$

with  $r_{\perp}^2 = x^2 + y^2$ . In principle these values can be directly compared with experimental data. However, it is more convenient to transform these quantities into dimensionless



deformation parameters  $\beta_2$  and  $\beta_3$  using the relations

$$Q_{20} = \sqrt{\frac{16\pi}{5}} \frac{3}{4\pi} Z R_0^2 \beta_2, \quad (7)$$

$$Q_{30} = \sqrt{\frac{16\pi}{7}} \frac{3}{4\pi} Z R_0^3 \beta_3, \quad (8)$$

where  $R_0 = 1.2A^{1/3}$ . These deformation parameters are more frequently used in experimental works than quadrupole and octupole moments. In addition, the potential energy surfaces (PES) are plotted in this paper in the  $(\beta_2, \beta_3)$  deformation plane.

In order to avoid the uncertainties connected with the definition of the size of the pairing window [40], we use the separable form of the finite range Gogny pairing interaction introduced by Tian *et al.* [41]. Its matrix elements in  $r$ -space have the form

$$V(\mathbf{r}_1, \mathbf{r}_2, \mathbf{r}'_1, \mathbf{r}'_2) = -G\delta(\mathbf{R} - \mathbf{R}')P(r)P(r')\frac{1}{2}(1 - P^\sigma), \quad (9)$$

with  $\mathbf{R} = (\mathbf{r}_1 + \mathbf{r}_2)/2$  and  $\mathbf{r} = \mathbf{r}_1 - \mathbf{r}_2$  being the center-of-mass and relative coordinates. The form factor  $P(r)$  is of Gaussian shape,

$$P(r) = \frac{1}{(4\pi a^2)^{3/2}} e^{-r^2/4a^2}. \quad (10)$$

The two parameters  $G = 728 \text{ MeV fm}^3$  and  $a = 0.644 \text{ fm}$  of this interaction are the same for protons and neutrons and were derived in Ref. [41] by a mapping of the  $^1S_0$  pairing gap of infinite nuclear matter to that of the Gogny force D1S [42]. This pairing provides a reasonable description of pairing properties in the actinides (see Refs. [23,34,43]) and was used in our previous studies of octupole deformation in Ref. [4].<sup>1</sup>

The potential energy surfaces are calculated in constrained calculations in the  $(\beta_2, \beta_3)$  plane for the  $\beta_2$  values ranging from  $-0.2$  up to  $0.4$  (ranging from  $-0.6$  up to  $0.2$ ) if the ground state has prolate (oblate) deformation in the calculations of Ref. [27] and for the  $\beta_3$  values ranging from  $0.0$  up to  $0.3$  with a deformation step of  $0.02$  in each direction. The energies of the local minima are defined in unconstrained calculations.

The effect of octupole deformation can be quantitatively characterized by the quantity  $\Delta E_{\text{oct}}$ , defined as

$$\Delta E_{\text{oct}} = E^{\text{oct}}(\beta_2, \beta_3) - E^{\text{quad}}(\beta'_2, \beta'_3 = 0), \quad (11)$$

where  $E^{\text{oct}}(\beta_2, \beta_3)$  and  $E^{\text{quad}}(\beta'_2, \beta'_3 = 0)$  are the binding energies of the nucleus in two local minima of the potential energy surface; the first minimum corresponds to octupole deformed shapes and second one to the shapes with no octupole deformation. The quantity  $|\Delta E_{\text{oct}}|$  represents the gain of binding due to octupole deformation. It is also an indicator of the stability of the octupole deformed shapes. Large  $|\Delta E_{\text{oct}}|$  values are typical for well pronounced octupole minima in

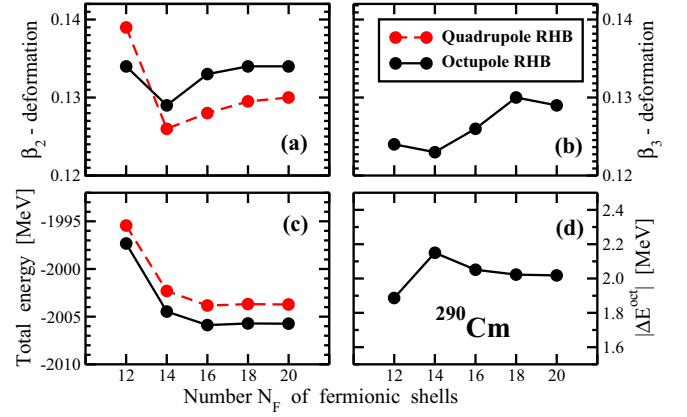


FIG. 1. The dependence of calculated quadrupole and octupole deformations, total binding energy and the  $|\Delta E^{\text{oct}}|$  quantity on the number of fermionic shells employed in the RHB calculations for  $^{290}\text{Cm}$  with the DD-PC1 functional. The results obtained in octupole and quadrupole RHB codes in respective local minima with  $(\beta_2 \neq 0, \beta_3 \neq 0)$  and  $(\beta_2 \neq 0, \beta_3 = 0)$  are shown by solid black and dashed red curves, respectively.

the PES; for such systems the stabilization of static octupole deformation is likely. In contrast, small  $|\Delta E_{\text{oct}}|$  values are characteristic for soft (in octupole direction) PES typical for octupole vibrations. In such systems beyond-mean-field effects can play an important role (see Ref. [4] and references quoted therein).

The truncation of the basis is performed in such a way that all states belonging to the major shells up to  $N_F = 16$  ( $N_F = 18$  for superheavy  $Z > 106$  nuclei) fermionic shells for the Dirac spinors and up to  $N_B = 20$  bosonic shells for the meson fields in the case of meson exchange functionals are taken into account. The dependence of the calculated quantities on  $N_F$  is illustrated in Fig. 1. One can see that all physical quantities of interest saturate with increasing  $N_F$ . The comparison of the results shows that the calculations with  $N_F = 16$  reproduce the results of the  $N_F = 20$  truncation scheme with an accuracy of 0.007% or better for binding energies, 1.6% for the  $|\Delta E^{\text{oct}}|$  quantity, 1.56% or better for quadrupole deformations, and 2.3% for octupole deformation. Somewhat increased errors for deformations are the consequences of the softness of the potential energy surface; for such PES some drift in the calculated equilibrium deformation is possible with little impact on total binding energy. Note that a larger basis with  $N_F = 18$  is used for superheavy nuclei with  $Z > 106$ . This increase of the basis fully compensates for the increase of the proton number in the system. As a result, similar or better accuracy of the description of physical observables is obtained in superheavy nuclei. Thus, we conclude that the employed truncation of the basis provides sufficient numerical accuracy of the calculations in the vicinity of the normal deformed minimum.

### III. THE PROPERTIES OF OCTUPOLE DEFORMED NUCLEI AND THEIR DEPENDENCE ON THE COVARIANT ENERGY DENSITY FUNCTIONAL

The global search for octupole deformed nuclei was performed for all even-even  $Z = 88$ –126 nuclei from the

<sup>1</sup>By mistake the parameters  $G = 738 \text{ MeV fm}^3$  and  $a = 0.636 \text{ fm}$ , derived from the D1 Gogny force [41], are quoted in Ref. [4]. In reality, the same parameters  $G = 728 \text{ MeV fm}^3$  and  $a = 0.644 \text{ fm}$  as the ones employed in the present paper are used in the calculations of Ref. [4].



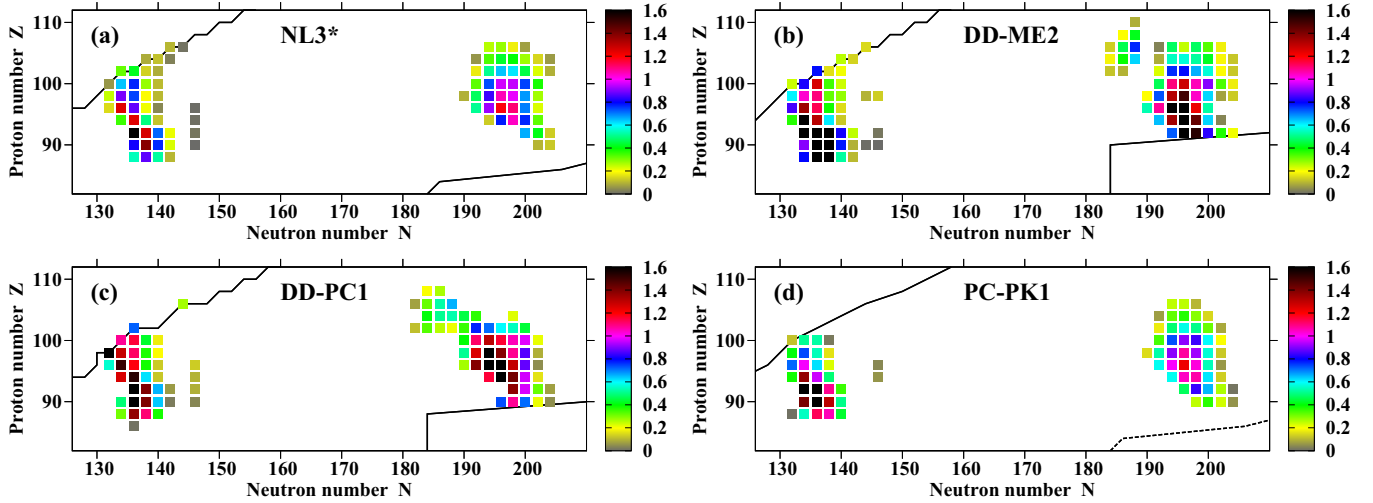


FIG. 2. Octupole deformed nuclei in the selected part of the nuclear chart. Only nuclei with nonvanishing  $\Delta E^{\text{oct}}$  are shown by squares; the colors of the squares represent the values of  $|\Delta E^{\text{oct}}|$  (see colormap). The two-proton and two-neutron drip lines are displayed by solid black lines; for the CEDFs NL3\*, DD-ME2, and DD-PC1 they are taken from Ref. [34]. Two-proton drip line for PC-PK1 is taken from Ref. [27]. The two-neutron drip line of the NL3\* functional is used in panel (d) since it is not defined for CEDF PC-PK1 at present.

two-proton drip line up to either neutron number  $N = 210$  or the two-neutron drip line (whichever comes first in neutron number) employing CEDFs NL3\*, DD-ME2, DD-PC1, and PC-PK1. Note that we use here the results obtained with CEDFs NL3\* and DD-PC1 in Ref. [4] for the  $Z = 88\text{--}106$  nuclei. Contrary to the results obtained within the microscopic+macroscopic approach in Ref. [25] and HFB calculations with Gogny D1S force in Ref. [26], our calculations do not reveal the presence of octupole deformation in the ground states of superheavy nuclei with  $Z \geq 110$ . This issue will be discussed later in detail in Sec. V.

Figure 2 shows the summary of the nuclei which possess octupole deformation in the ground state. The  $Z \sim 92$ ,  $N \sim 136$  actinides were studied previously in detail in Ref. [4] and they are shown here only for comparison with the  $Z \sim 96$ ,  $N \sim 196$  region of octupole deformation. In both regions, the number of even-even nuclei with calculated nonzero octupole deformation depends on the employed functional. There are 47 (44), 57 (38), 47 (31), and 64 (46) of such nuclei in the  $Z \sim 96$ ,  $N \sim 196$  ( $Z \sim 92$ ,  $N \sim 136$ ) region of octupole deformation in the calculations with the NL3\*, DD-PC1, PC-PK1, and DD-ME2 functionals, respectively. Thus, the calculations with CEDFs DD-ME2 and PC-PK1 confirm earlier CDFT predictions on the existence of new region of octupole deformation centered around  $Z \sim 96$ ,  $N \sim 196$  obtained with the CEDFs NL3\* and DD-PC1 in Ref. [4]. Most of the functionals predict that this region is substantially larger than the one around  $Z \sim 92$ ,  $N \sim 136$ . Moreover, the maximum gain in binding due to octupole deformation is comparable in the  $Z \sim 96$ ,  $N \sim 196$  and  $Z \sim 92$ ,  $N \sim 136$  regions. This strongly suggests the stabilization of octupole deformation in the nuclei belonging to the central part of the  $Z \sim 96$ ,  $N \sim 196$  region.

The detailed information on calculated equilibrium quadrupole ( $\beta_2$ ) and octupole ( $\beta_3$ ) deformations as well as the gains ( $\Delta E^{\text{oct}}$ ) in binding due to octupole deformation is

summarized in Fig. 3. These results show large similarities between the NL3\* and PC-PK1 functionals on the one hand and the DD-ME2 and DD-PC1 functionals on the other hand. The first pair of functionals typically shows somewhat smaller gain in binding due to octupole deformation as compared with second one. This is likely due to the fact that the pairing is stronger in neutron rich nuclei for the first pair of the functionals as compared with second one (see Ref. [36]); strong pairing leads to the reduction of  $|\Delta E^{\text{oct}}|$  (see Sec. V of Ref. [4]). The differences or similarities in underlying shell structure could be another source of observed features.

For all functionals the maximum of the gain in binding energy due to octupole deformation takes place around  $Z \sim 96$ ,  $N \sim 196$ . For nuclei in the vicinity of these particle numbers there is very little dependence of calculated equilibrium deformations on the employed functional. However, on going away from these particle numbers the differences in calculated deformations increase because the nuclei become more soft in octupole deformation and thus more transitional in nature (see the discussion in Sec. IV). In particular, the particle numbers at which the transition from quadrupole deformed to octupole deformed shapes takes place become strongly dependent on the employed functional.

Two  $Z = 108$  (two  $Z = 108$  and one  $Z = 110$ ) nuclei have nonzero octupole deformation in the calculations with CEDF DD-PC1 (DD-ME2) [see Figs. 2(b) and 2(c)]. They are not shown in Fig. 3 since all these nuclei are extremely soft in octupole deformation with very small gain in binding energy due to octupole deformation ( $|\Delta E^{\text{oct}}| < 0.1$  MeV).

#### IV. EVOLUTION OF POTENTIAL ENERGY SURFACES WITH PARTICLE NUMBERS: AN EXAMPLE OF THE DD-PC1 FUNCTIONAL

In order to better understand the evolution and development of octupole deformation with particle number, the potential



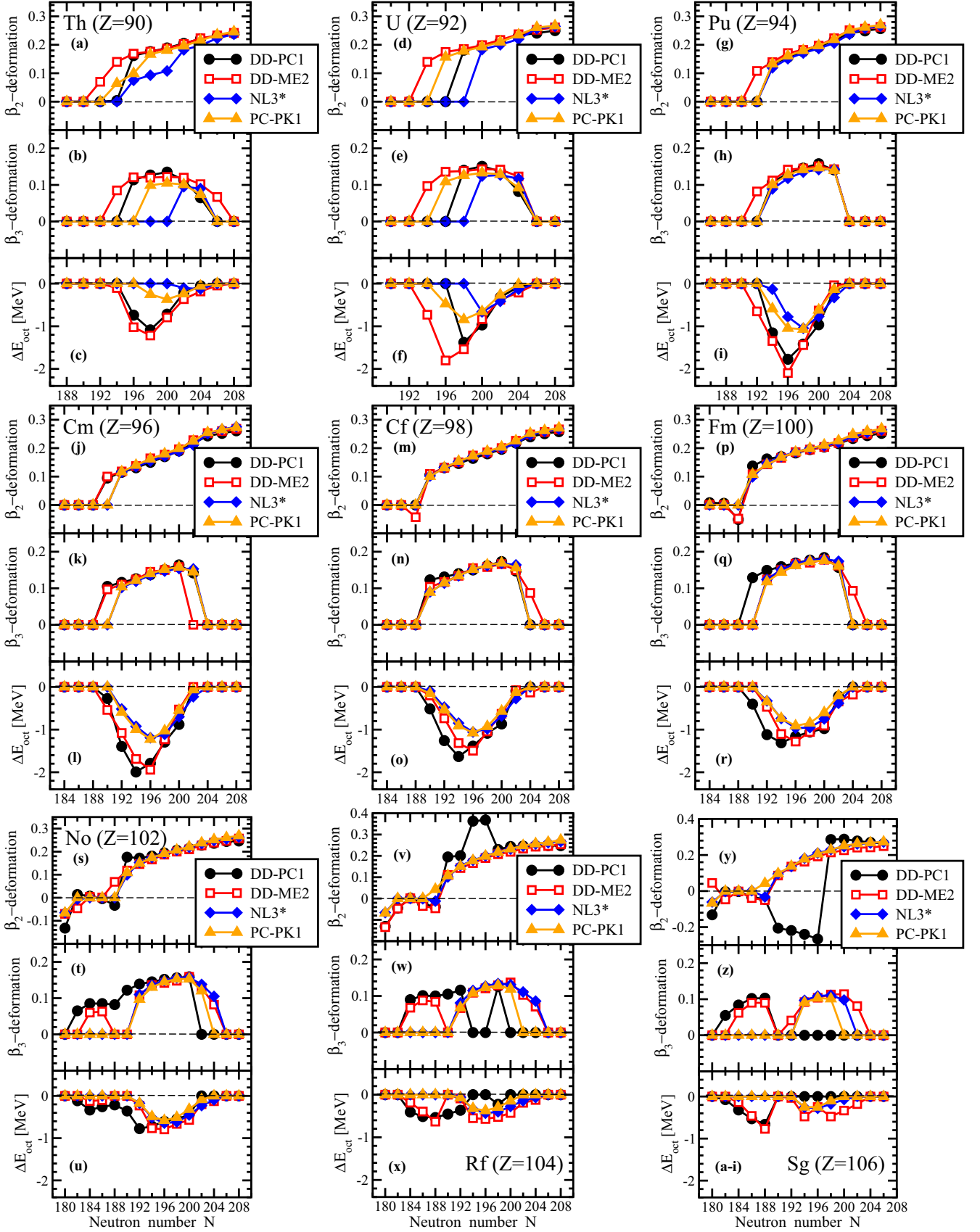


FIG. 3. The calculated equilibrium quadrupole  $\beta_2$  (top panel of each figure) and octupole  $\beta_3$  (middle panel of each figure) deformations as well as the  $\Delta E_{\text{oct}}$  quantities (bottom panel of each figure). The employed functionals are indicated.



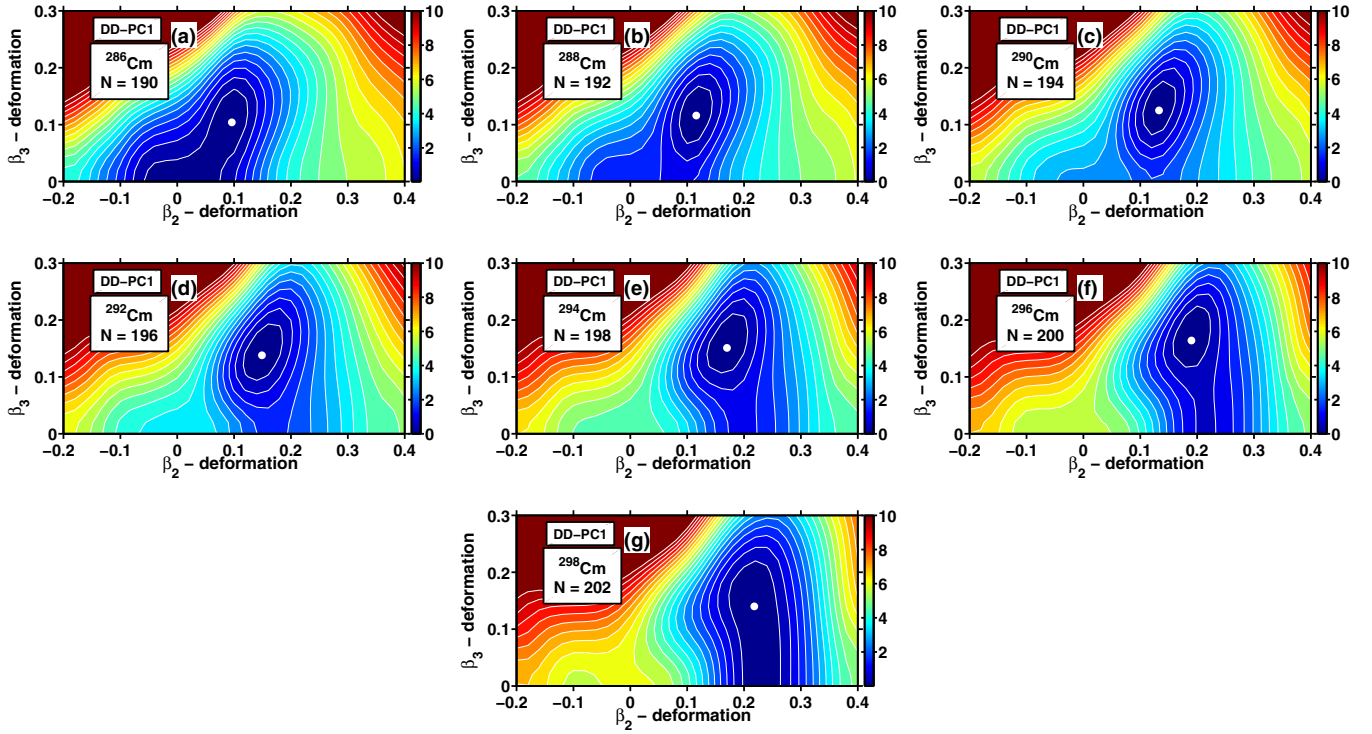


FIG. 4. Potential energy surfaces of the Cm ( $Z = 96$ ) isotopes in the  $(\beta_2, \beta_3)$  plane calculated with the CEDF DD-PC1. The white circle indicates the global minimum. Equipotential lines are shown in steps of 0.5 MeV. The neutron number  $N$  is shown in each panel in order to make the comparison between different isotones easier.

energy surfaces (PES) of the Cm ( $Z = 96$ ) isotopes and  $N = 198$  isotones obtained in the RHB calculations with CEDF DD-PC1 are shown in Figs. 4 and 5. The center of the

crossing in the  $(Z, N)$  plane represented by the  $^{294}\text{Cm}$  nucleus is located in the region of maximum gain of binding due to octupole deformation (see Fig. 2).

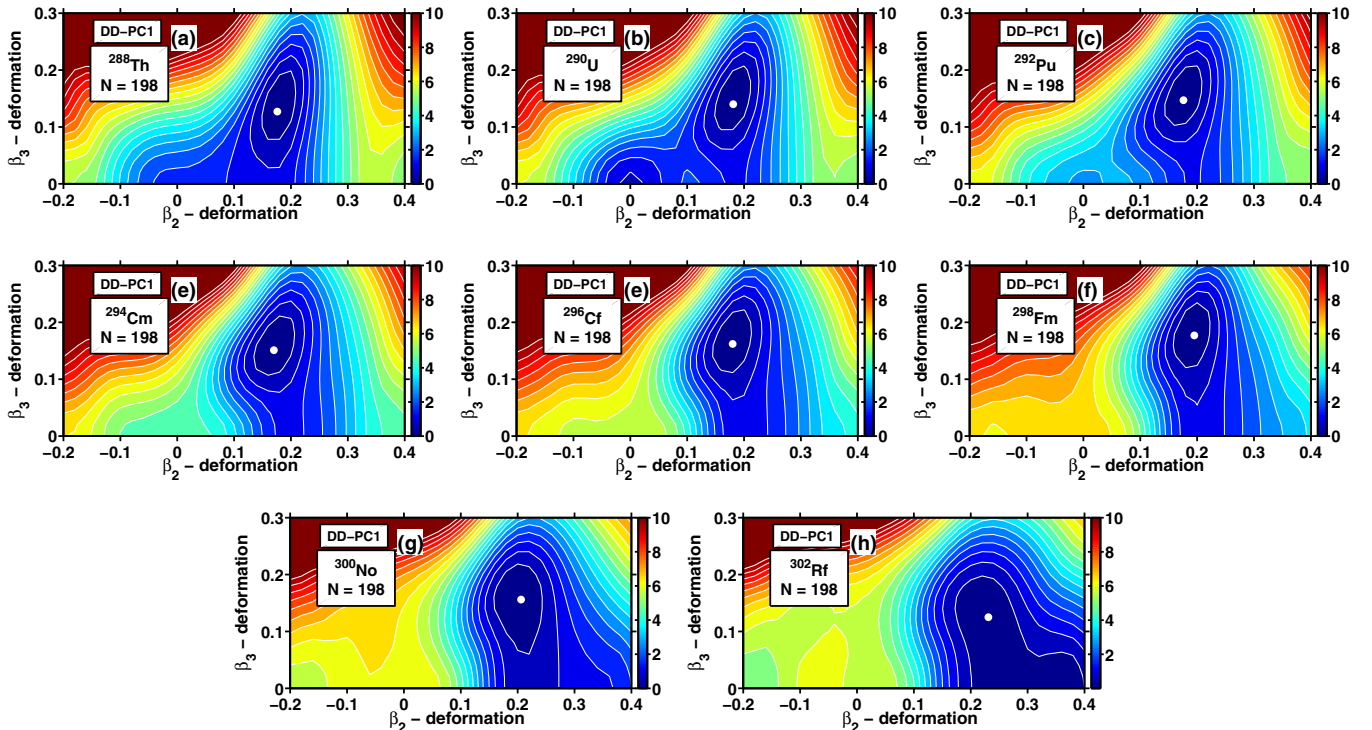


FIG. 5. The same as Fig. 4, but for the  $N = 198$  isotones.



The PES of the  $^{286}\text{Cm}$  nucleus are rather soft in the  $\beta_3$  direction, with the gain in binding due to octupole deformation being  $|\Delta E_{\text{oct}}| = 0.271$  MeV. The addition of the neutrons leads to the stabilization of octupole deformation in the  $^{288-294}\text{Cm}$  isotopes, with the largest gains in binding due to octupole deformation being 1.994 and 1.790 MeV in the  $^{290}\text{Cm}$  and  $^{292}\text{Cm}$  nuclei, respectively. Subsequent increase of the neutron number leads to the softening of potential energy surfaces so that  $|\Delta E_{\text{oct}}|$  is rather small (0.049 MeV) in the  $^{298}\text{Cm}$  nucleus.

The PES for the  $N = 198$  isotones are displayed in Fig. 5. One can see that the lowest  $Z$  nucleus ( $^{288}\text{Th}$  with  $Z = 88$ ) shown in this figure already has a well pronounced minimum in octupole deformation which is characterized by  $|\Delta E_{\text{oct}}| = 1.084$  MeV. This is because the  $^{286}\text{Rn}$  nucleus with lower  $Z$  value ( $Z = 86$ ), which is expected to be more octupole soft, is located beyond the two-neutron drip line (see Fig. 2). The  $^{290}\text{U}$ ,  $^{292}\text{Pu}$ ,  $^{294}\text{Cm}$ ,  $^{296}\text{Cf}$ , and  $^{298}\text{Fm}$  nuclei have well pronounced octupole minima in the PES. The largest gain in binding due to octupole deformation,  $|\Delta E_{\text{oct}}| = 1.419$  MeV, is reached in the  $^{292}\text{Pu}$  nucleus. Subsequent increase of proton number above  $Z = 100$  gradually decreases  $|\Delta E_{\text{oct}}|$  so that PES surface becomes very soft in  $^{302}\text{Rf}$ .

## V. ASSESSING SYSTEMATIC UNCERTAINTIES IN MODEL PREDICTIONS

All theoretical approaches to nuclear many body problem are based on some approximations. For example, in the DFT framework, there are two major sources of these approximations, namely, the range of interaction and the form of the density dependence of the effective interaction [44,45]. In the nonrelativistic case one has zero range Skyrme and finite range Gogny forces and different density dependencies [44]. A similar situation exists also in the relativistic case: point coupling and meson exchange models have an interaction of zero and of finite range, respectively [9,30–32]. The density dependence is introduced either through an explicit dependence of the coupling constants [31,32,46] or via nonlinear meson couplings [30,45]. This ambiguity in the definition of the range of the interaction and its density dependence leads to several major classes of the covariant energy density functionals, which were discussed in detail in Ref. [34].

These approximations lead to theoretical uncertainties in the description of physical observables. While in known nuclei these uncertainties could be minimized by benchmarking the model description to experimentally known nuclei (for example, via the fitting protocol), they grow in magnitude when we extrapolate beyond known regions [34,47]. In such a situation, the estimate of theoretical uncertainties is needed. This issue was discussed in detail in Refs. [47,48] and in the context of global studies within CDFT in the introduction of Ref. [34] and in Ref. [37]. In the CDFT framework, systematic theoretical uncertainties and their sources have been studied globally for the ground state masses, deformations, charge radii, neutrons skins, positions of drip lines, etc. in Refs. [4,27,34–36,49] and for inner fission barriers in superheavy nuclei in Ref. [37].

In the present paper, we focus on the uncertainties related to the choice of the energy density functional. Similar to our previous studies ([4,27,34,36,37]), we define systematic

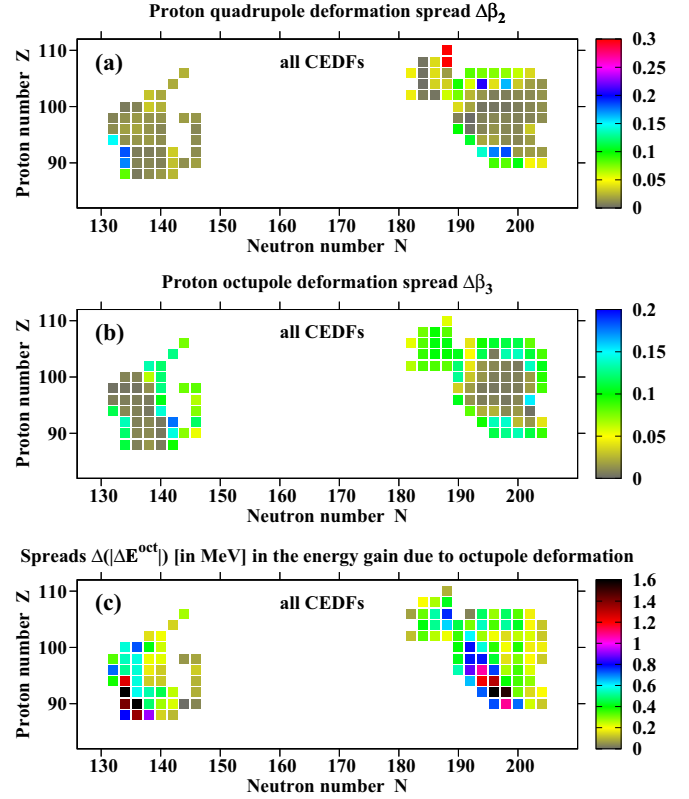


FIG. 6. The calculated spreads in quadrupole and octupole deformations as well as in the  $|\Delta E^{\text{oct}}|$  quantities. The nucleus is shown by a square if it has nonzero octupole deformation in the calculations with at least one CEDF.

theoretical uncertainty for a given physical observable (which we call in the following “spreads”) via the spread of theoretical predictions as [34]

$$\Delta O(Z, N) = |O_{\text{max}}(Z, N) - O_{\text{min}}(Z, N)|, \quad (12)$$

where  $O_{\text{max}}(Z, N)$  and  $O_{\text{min}}(Z, N)$  are the largest and smallest values of the physical observable  $O(Z, N)$  obtained within the set of CEDFs under investigation for the  $(Z, N)$  nucleus.

These spreads for the calculated quadrupole and octupole deformations as well as for the  $|\Delta E^{\text{oct}}|$  quantity are shown in Fig. 6. One can see that the spreads for the  $\beta_2$  and  $\beta_3$  deformations in the central parts of the  $Z \sim 96$ ,  $N \sim 196$  and  $Z \sim 92$ ,  $N \sim 136$  regions are small. They increase at the boundaries of these regions where the PES of the nuclei are soft in octupole deformation. As a result, model predictions become strongly dependent on fine details of underlying single-particle structure so that the same  $(Z, N)$  nucleus could be octupole deformed in one functional but only quadrupole deformed in another functional (see Fig. 2). A similar situation with low reliability of theoretical predictions in some parts of the nuclear chart has been seen in the transitional regions between quadrupole deformed and spherical shapes (see Figs. 18 and 20 in Ref. [34]) in the axial RHB calculations restricted to reflection symmetric shapes. The  $Z = 108, 110$  nuclei with  $N = 188$  show very large spreads in quadrupole deformation [Fig. 6(a)]. These two nuclei are octupole deformed with



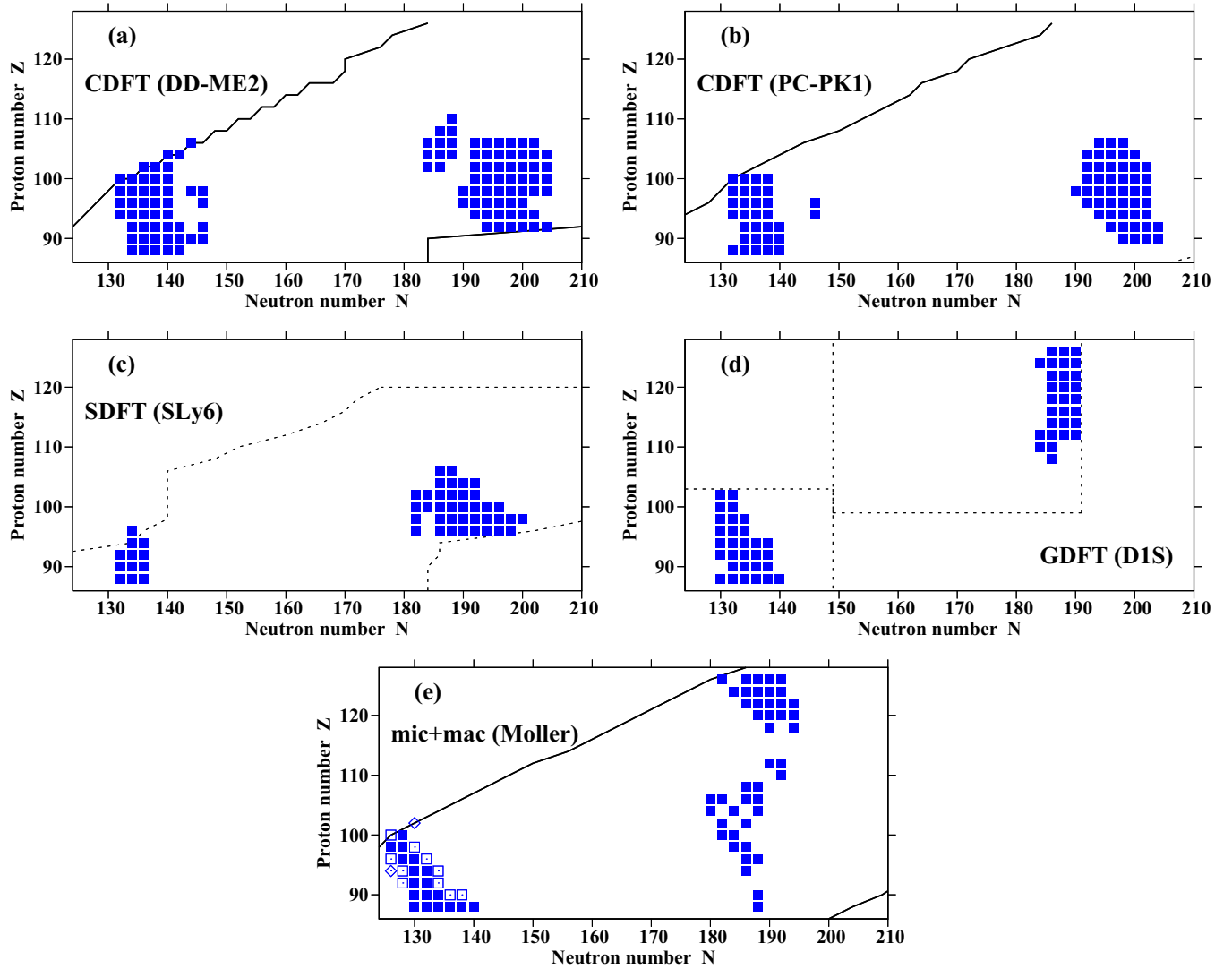


FIG. 7. Octupole deformed nuclei obtained in the CDFT calculations with CEDFs DD-ME2 (a) and PC-PK1 (b), in Skyrme DFT calculations with the SLy6 functional [50] (c), Gogny DFT calculations with EDF D1S [3,26] (d), and in microscopic+macroscopic calculations of Ref. [2,25] (e). Only nuclei with nonzero calculated octupole deformation are shown by squares. The two-proton and two-neutron drip lines are displayed by solid black lines in panels (a), (b), and (e). In panels (c) and (d), the regions in which the searches for octupole deformation were performed are outlined by dashed lines. The results of the SDFT calculations for the  $Z \sim 100$ ,  $N \sim 190$  region of octupole deformation are extracted from Fig. 11 of Ref. [50]. The  $Z \sim 92$ ,  $N \sim 134$  region of octupole deformation in panel (c) is shown schematically (based on Fig. 4 of Ref. [50]). Note that the results presented in panel (d) in two regions of octupole deformation were obtained in two independent calculations of Refs. [3,26]. The nuclei which are octupole deformed in the mic+mac calculations of Ref. [25] are shown by solid blue squares and open diamonds in panel (e). Open squares indicate additional (as compared with Ref. [25]) octupole deformed nuclei obtained in Ref. [2], while open diamonds indicate the nuclei which cease to be octupole deformed (as compared with Ref. [25]) in the mic+mac calculations of Ref. [2].

$\beta_2 \sim -0.045$ ,  $\beta_3 \sim 0.07$  only in the calculations with the DD-ME2 functional. However, they are spherical in the calculations with CEDFs NL3\* and PC-PK1 but oblate (with  $\beta_2 \sim -0.36$ ) in the calculations with DD-PC1 (see Fig. 6 in Ref. [27]).

Systematic theoretical uncertainties for the energy gain due to octupole deformation are shown in Fig. 6(c). These uncertainties show a different pattern in the  $(Z, N)$  plane as compared with the uncertainties for the  $\beta_2$  and  $\beta_3$  deformations [Figs. 6(a) and 6(b)]. The maximum uncertainties for the  $|\Delta E^{\text{oct}}|$  quantity exist in the left bottom corners of the

$Z \sim 96$ ,  $N \sim 196$  and  $Z \sim 92$ ,  $N \sim 136$  regions of octupole deformation. Theoretical uncertainties gradually decrease on going away from these corners and become quite small at the boundaries of the regions of octupole deformation. This is not surprising considering the fact that the nuclei at these boundaries are octupole soft with rather small gain in binding due to octupole deformation.

It is important to compare the CDFT predictions for the  $Z \sim 96$ ,  $N \sim 196$  region of octupole deformation with the ones obtained in nonrelativistic theories. Such a comparison is presented in Fig. 7 where two extreme CDFT predictions



for octupole deformed region [the largest (smallest)  $Z \sim 96$ ,  $N \sim 196$  region of octupole deformation is obtained in the calculations with DD-ME2 (PC-PK1) functional] in the indicated part of nuclear chart are compared with the predictions obtained in the Skyrme and Gogny DFTs and macroscopic+microscopic approach. The Skyrme DFT calculations with the SLy6 functional predict such a region with the center located around  $Z = 100$ ,  $N = 190$  [50] [see Fig. 7(c)]. A similar region of octupole deformation (but with smaller gain in binding energy due to octupole deformation) was also obtained in the calculations with the SV-min EDF [50]. The Gogny DFT calculations are limited to the  $(Z, N)$  plane [see Fig. 7(d)]; even then they do not indicate the presence of octupole deformation in the nuclei located in the upper parts of the regions of octupole deformation obtained in the Skyrme and CDFT calculations. However, the extension of the Gogny DFT calculations to the  $Z = 90$ –108,  $N = 180$ –210 region of nuclear chart is needed to clarify the question of the existence of the  $Z \sim 96$ ,  $N \sim 196$  region of octupole deformation in this type of EDF. In contrast, the mic+mac calculations of Ref. [25] predict the existence of octupole deformation in this region [Fig. 7(e)]. However, the island of octupole deformation is smaller than the one obtained in the CDFT or Skyrme DFT calculations and it is centered around  $Z = 100$ ,  $N = 184$ . It is necessary to mention that that these results were obtained more than twenty years ago. Newer mic+mac calculations of Ref. [2] do not cover this part of the nuclear chart. However, in the  $Z \sim 92$ ,  $N \sim 134$  region of octupole deformation, the number of octupole deformed even-even nuclei is increased from 20 in Ref. [25] to 27 in Ref. [2]. It would be interesting to see how the number of octupole deformed nuclei in the  $Z \sim 100$ ,  $N \sim 184$  region would be modified if the newer formalism of the mic+mac approach of Ref. [2] with improved model parameters would be applied to this region.

Despite placing the center of the island of octupole deformed nuclei at different particle numbers (at  $Z \sim 96$ ,  $N \sim 196$  in CDFT, at  $Z \sim 100$ ,  $N \sim 190$  in Skyrme DFT and at  $Z \sim 100$ ,  $N \sim 184$  in the mic+mac approach), modern theories agree on the existence of such islands in neutron-rich

actinides and low- $Z$  superheavy nuclei. However, their predictions diverge for the  $Z \geq 110$  superheavy nuclei. The CDFT calculations of the present paper and the Skyrme DFT calculations of Ref. [50] do not predict the existence of octupole deformation in the ground states of the  $110 \leq Z \leq 126$  and  $110 \leq Z \leq 120$  superheavy nuclei, respectively. In contrast, the Gogny DFT (Fig. 7(d) and Ref. [26]) and mic+mac (Fig. 7(e) and Ref. [25]) calculations predict the existence of such nuclei. The HFB calculations based on the Gogny D1S force predict octupole deformation in the ground states of the  $(Z = 108$ –126,  $N = 186$ –190) even-even nuclei (see Fig. 3 in Ref. [26]). These nuclei either do not have quadrupole deformation (the  $N = 186$  and some  $N = 188$  nuclei) or this deformation is rather small ( $\beta_2 < 0.1$ ) for  $N = 190$  and some  $N = 188$  nuclei. The octupole deformation is rather small for most of these nuclei apart of few  $N = 188$  nuclei and the majority of the  $N = 190$  nuclei which have substantial octupole deformation  $\beta_3$  exceeding 0.1. Note that these calculations cover only nuclei with  $N \leq 190$ . More extensive mic+mac calculations of Ref. [25] indicate a larger region of octupole deformation in the superheavy nuclei [see Fig. 7(e)].

The existence of octupole deformed shapes is dictated by the underlying shell structure. Strong octupole coupling exists for particle numbers associated with a large  $\Delta N = 1$  interaction between intruder orbitals with  $(l, j)$  and normal-parity orbitals with  $(l - 3, j - 3)$  [1]. Thus, the differences discussed above in the model predictions are traced back to the differences in the underlying single-particle structure. For normal deformed nuclei not far away from beta stability the tendency towards octupole deformation or strong octupole correlations occurs just above closed shells. For example, in the CDFT the maximum of octupole correlations takes place in the  $A \sim 230$  region of octupole deformation at proton number  $Z \sim 92$  (the coupling between the proton  $1i_{13/2}$  and  $2f_{7/2}$  orbitals) and  $N \sim 136$  (the coupling between the neutron  $1j_{15/2}$  and  $2g_{9/2}$  orbitals). In the  $Z \sim 96$ ,  $N \sim 196$  region, the presence of octupole deformation is due to the interaction of the  $2h_{11/2}$  and  $1k_{17/2}$  neutron orbitals and of the  $1i_{13/2}$  and

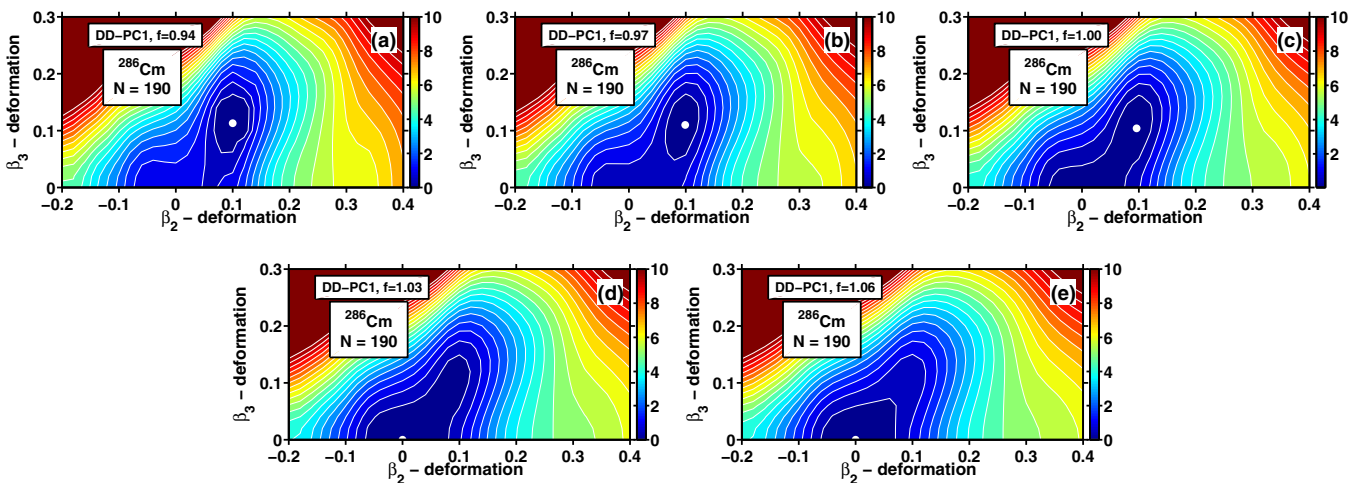
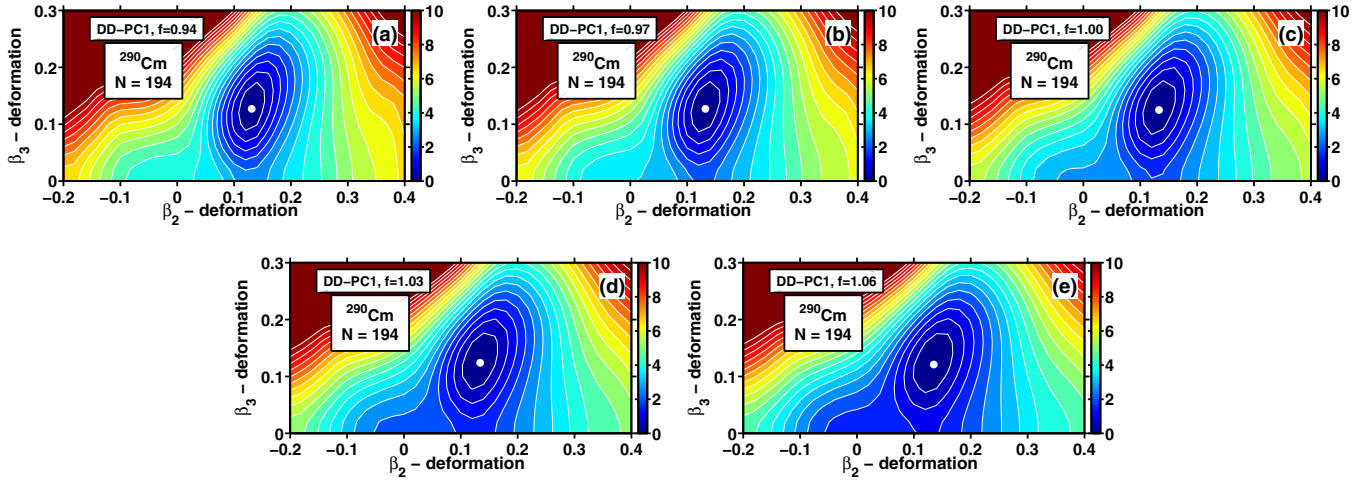


FIG. 8. Potential energy surfaces of  $^{286}\text{Cm}$  in the  $(\beta_2, \beta_3)$  plane calculated with the CEDF DD-PC1 for different values of scaling factor  $f$  of the pairing strength. The white circle indicates the global minimum. Equipotential lines are shown in steps of 0.5 MeV.



FIG. 9. The same as Fig. 8, but for  $^{290}\text{Cm}$ .

$2f_{7/2}$  proton orbitals. Note that the maximum of the interaction of proton orbitals occurs at a higher proton number  $Z$  as compared with the well known  $A \sim 230$  region of octupole deformation in actinides. In the  $Z \sim 120$ ,  $N \sim 190$  region, the interactions of the  $2h_{11/2}$  and  $1k_{17/2}$  neutron orbitals and of the  $1j_{15/2}$  and  $2g_{9/2}$  proton orbitals are responsible for strong octupole correlations in the Gogny DFT and mic+mac calculations. However, the energies of these states and their positions with respect of the Fermi level are described differently in different models (see, for example, Figs. 1, 4, 9, and 15 in Ref. [12], Fig. 4 in Ref. [51], and Fig. 1 in Ref. [27]).

The predictive power of the above-discussed models in the description of these energies and, as a consequence, of the regions of octupole deformation, decreases on going away from the known region of nuclear chart. Some differences in the predictions of the region of octupole deformation do already exist for the known  $A \sim 230$  region of octupole deformation (see Fig. 7 and the discussion in Ref. [4]). However, they become magnified with increasing neutron number up to  $N \sim 196$  on going to the  $Z \sim 96$ ,  $N \sim 196$  region of octupole deformation and especially pronounced with an additional increase of neutron number up to  $Z \sim 120$ . In the  $Z \sim 120$ ,  $N \sim 190$  region, there are substantial discrepancies in model predictions. Note that in this region of nuclear chart the state-of-the-art theories disagree even in the prediction of large spherical shell gaps and thus of the properties of superheavy nuclei [12,27,52].

## VI. THE IMPACT OF PAIRING STRENGTH CHANGES

The extrapolations beyond the known region of nuclei are associated with theoretical uncertainties. The systematic uncertainties related to the form of the functional were quantified in Sec. V; note that they are related to the particle-hole channel of the DFTs. In addition, there are the uncertainties in the particle-particle (pairing) channel; they are expected to become especially large in the vicinity of the two-neutron drip line (see Refs. [49,53]). The study of  $^{218-234}\text{Th}$  isotopes in Sec. V of Ref. [4] showed that in general pairing counteracts the shell effects. As a result, the strongest trend towards octupole

deformation is seen in the systems with no pairing, while the increase of pairing suppresses it. The modification of the pairing strength may also lead to the changes in the topology of potential energy surfaces.

As illustrated in Figs. 8 and 9 these features are also present in neutron-rich actinides. The  $^{286}\text{Cm}$  and  $^{290}\text{Cm}$  nuclei are used here as the examples and the scaling factor  $f$  of the pairing strength is varied in the indicated range. This is a factor by which the matrix elements of Eq. (9) are multiplied. Based on previous studies of the pairing in the CDFT framework in Refs. [23,49], the variations of the scaling factor in the range of  $\pm 3\%$  with respect to  $f = 1.0$  should be considered very reasonable, but still larger variations could not be excluded. The  $^{286}\text{Cm}$  nucleus, located at the borderline of the octupole deformed region [see Fig. 2(c)], is characterized by PES which is extremely soft in the octupole direction [Fig. 8(c)].  $^{290}\text{Cm}$  is located at the center of the island of octupole deformation [Fig. 2(c)] and is characterized by a deep octupole minimum with large  $|\Delta E^{\text{oct}}| \sim 2.0$  MeV [see Fig. 1(d)]. The impacts of the scaling factor  $f$  changes on the gain in binding due to octupole deformation and on equilibrium deformations are summarized in Tables I and II, respectively. Similar to the results presented in Sec. V of Ref. [4], the reduction of pairing strength leads to a more pronounced octupole minimum in both nuclei. In contrast, the increase of pairing strength reduces the depth of the octupole minimum in  $^{290}\text{Cm}$  and makes the  $^{286}\text{Cm}$  nucleus spherical. Thus, one can conclude that weaker (stronger) pairing would make the island of octupole deformation broader (narrower) with more (less) pronounced gains in binding due to octupole deformation in nuclei. The

TABLE I. The gain in binding  $|\Delta E^{\text{oct}}|$  (in MeV) due to octupole deformation calculated for different values of scaling factor  $f$  of the pairing.

Nucleus	$f = 0.94$	$f = 0.97$	$f = 1.00$	$f = 1.03$	$f = 1.06$
$^{286}\text{Cm}$	1.089	0.696	0.271	0.0	0.0
$^{290}\text{Cm}$	2.680	2.363	1.994	1.735	1.434



TABLE II. The  $(\beta_2, \beta_3)$  deformations of the minimum of PES obtained in the RHB calculations with different values of scaling factor  $f$ .

Nucleus	$f = 0.94$	$f = 0.97$	$f = 1.00$	$f = 1.03$	$f = 1.06$
$^{286}\text{Cm}$	0.100, 0.113	0.099, 0.110	0.095, 0.105	0.00, 0.00	0.00, 0.00
$^{290}\text{Cm}$	0.131, 0.127	0.132, 0.127	0.131, 0.126	0.134, 0.124	0.135, 0.121

impact of the modification of the pairing strength on the equilibrium deformation is small in  $^{290}\text{Cm}$ . A similar situation exists also in  $^{286}\text{Cm}$  for  $f = 0.94$ – $1.00$ . However, further increase of  $f$  triggers a transition to spherical shape.

## VII. CONCLUSIONS

A systematic search for axial octupole deformation was performed in the actinides and superheavy nuclei for proton numbers  $Z = 88$ – $126$  and neutron numbers from the two-proton drip line up to  $N = 210$  using four state-of-the-art covariant energy density functionals. Systematic theoretical uncertainties in the description of physical observables of octupole deformed nuclei were estimated. The main results can be summarized as follows:

- (1) The present CDFT investigation confirms our earlier predictions on the existence of the region of octupole deformation centered around  $Z \sim 96$ ,  $N \sim 196$  obtained with the DD-PC1 and NL3\* functionals [4]. Most of the CEDFs predict the size of this region in the  $(Z, N)$  plane to be larger than the one at  $Z \sim 92$ ,  $N \sim 136$ . On the other hand, the impacts of octupole deformation on the binding energies of the nuclei in these two regions are comparable. A similar region of octupole deformation is predicted also in Skyrme DFT [50] and mic+mac [25] calculations. However, it is centered at  $Z \sim 100$ ,  $N \sim 190$  in the Skyrme DFT calculations and at  $Z \sim 100$ ,  $N \sim 184$  in mic+mac calculations.

- (2) Systematic theoretical uncertainties in the predictions of quadrupole ( $\beta_2$ ) and octupole ( $\beta_3$ ) deformations as well as the gain in binding due to octupole deformation  $|\Delta E^{\text{oct}}|$  were quantified within the CDFT framework. They are comparable in the  $Z \sim 96$ ,  $N \sim 196$  and  $Z \sim 92$ ,  $N \sim 136$  regions of octupole deformation.
- (3) The search for octupole deformation in the ground states of even-even superheavy  $Z = 108$ – $126$  nuclei was performed in the CDFT framework for the first time. With the exception of two  $Z = 108$  (two  $Z = 108$  and one  $Z = 110$ ) octupole deformed nuclei in the calculations with CEDF DD-PC1 (DD-ME2), we do not find octupole deformed shapes in the ground states of these nuclei. These results are in agreement with the ones obtained in the Skyrme DFT but disagree with the ones obtained in Gogny DFT and mic+mac calculations. The latter calculations indicate the presence of large island of octupole deformed  $Z > 110$  nuclei centered around  $N \sim 190$ . These differences in the location of the islands of octupole deformed nuclei are due to the differences in the underlying single-particle structure.

## ACKNOWLEDGMENT

This material is based upon work supported by the U.S. Department of Energy, Office of Science, Office of Nuclear Physics under Grant No. DE-SC0013037.

- 
- [1] P. A. Butler and W. Nazarewicz, *Rev. Mod. Phys.* **68**, 349 (1996).
  - [2] P. Möller, R. Bengtsson, B. Carlsson, P. Olivius, T. Ichikawa, H. Sagawa, and A. Iwamoto, *At. Data Nucl. Data Tables* **94**, 758 (2008).
  - [3] L. M. Robledo and R. R. Rodríguez-Guzmán, *J. Phys. G* **39**, 105103 (2012).
  - [4] S. E. Agbemava, A. V. Afanasjev, and P. Ring, *Phys. Rev. C* **93**, 044304 (2016).
  - [5] H. Abusara, A. V. Afanasjev, and P. Ring, *Phys. Rev. C* **85**, 024314 (2012).
  - [6] N. Schunck and L. M. Robledo, *Rep. Prog. Phys.* **79**, 116301 (2016).
  - [7] S.-G. Zhou, *Phys. Scr.* **91**, 063008 (2016).
  - [8] M. Warda and L. M. Robledo, *Phys. Rev. C* **84**, 044608 (2011).
  - [9] D. Vretenar, A. V. Afanasjev, G. A. Lalazissis, and P. Ring, *Phys. Rep.* **409**, 101 (2005).
  - [10] P.-G. Reinhard, *Rep. Prog. Phys.* **52**, 439 (1989).
  - [11] P. Ring, *Prog. Part. Nucl. Phys.* **37**, 193 (1996).
  - [12] M. Bender, K. Rutz, P.-G. Reinhard, J. A. Maruhn, and W. Greiner, *Phys. Rev. C* **60**, 034304 (1999).
  - [13] E. V. Litvinova and A. V. Afanasjev, *Phys. Rev. C* **84**, 014305 (2011).
  - [14] A. V. Afanasjev and H. Abusara, *Phys. Rev. C* **81**, 014309 (2010).
  - [15] K. Rutz, J. A. Maruhn, P. G. Reinhard, and W. Greiner, *Nucl. Phys. A* **590**, 680 (1995).
  - [16] L. S. Geng, J. Meng, and H. Toki, *Chin. Phys. Lett.* **24**, 1865 (2007).
  - [17] Z. P. Li, B. Y. Song, J. M. Yao, D. Vretenar, and J. Meng, *J. Phys. G* **42**, 055109 (2015).
  - [18] K. Nomura, D. Vretenar, and B.-N. Lu, *Phys. Rev. C* **88**, 021303 (2013).
  - [19] K. Nomura, D. Vretenar, T. Nikšić, and B.-N. Lu, *Phys. Rev. C* **89**, 024312 (2014).
  - [20] J. M. Yao, E. F. Zhou, and Z. P. Li, *Phys. Rev. C* **92**, 041304 (2015).
  - [21] J. Zhao, B.-N. Lu, E.-G. Zhao, and S.-G. Zhou, *Phys. Rev. C* **86**, 057304 (2012).



- [22] J. Zhao, B.-N. Lu, E.-G. Zhao, and S.-G. Zhou, *Phys. Rev. C* **95**, 014320 (2017).
- [23] A. V. Afanasjev and O. Abdurazakov, *Phys. Rev. C* **88**, 014320 (2013).
- [24] A. V. Afanasjev, *Phys. Scr.* **89**, 054001 (2014).
- [25] P. Möller, J. R. Nix, W. D. Myers, and W. J. Swiatecki, *At. Data Nucl. Data Tables* **59**, 185 (1995).
- [26] M. Warda and J. L. Egido, *Phys. Rev. C* **86**, 014322 (2012).
- [27] S. E. Agbemava, A. V. Afanasjev, T. Nakatsukasa, and P. Ring, *Phys. Rev. C* **92**, 054310 (2015).
- [28] S. Goriely, A. Bauswein, and H.-T. Janka, *Astrophys. J.* **738**, L32 (2011).
- [29] O. Just, A. Bauswein, R. A. Pulpillo, S. Goriely, and H.-T. Janka, *Mon. Not. R. Astron. Soc.* **448**, 541 (2015).
- [30] G. A. Lalazissis, S. Karatzikos, R. Fossion, D. P. Arteaga, A. V. Afanasjev, and P. Ring, *Phys. Lett. B* **671**, 36 (2009).
- [31] G. A. Lalazissis, T. Nikšić, D. Vretenar, and P. Ring, *Phys. Rev. C* **71**, 024312 (2005).
- [32] T. Nikšić, D. Vretenar, and P. Ring, *Phys. Rev. C* **78**, 034318 (2008).
- [33] P. W. Zhao, Z. P. Li, J. M. Yao, and J. Meng, *Phys. Rev. C* **82**, 054319 (2010).
- [34] S. E. Agbemava, A. V. Afanasjev, D. Ray, and P. Ring, *Phys. Rev. C* **89**, 054320 (2014).
- [35] A. V. Afanasjev, S. E. Agbemava, D. Ray, and P. Ring, *Phys. Lett. B* **726**, 680 (2013).
- [36] A. V. Afanasjev and S. E. Agbemava, *Phys. Rev. C* **93**, 054310 (2016).
- [37] S. E. Agbemava, A. V. Afanasjev, D. Ray, and P. Ring, *Phys. Rev. C* **95**, 054324 (2017).
- [38] P. Ring and P. Schuck, *The Nuclear Many-Body Problem* (Springer-Verlag, Berlin, 1980).
- [39] P. Bonche, H. Flocard, and P. H. Heenen, *Comput. Phys. Commun.* **171**, 49 (2005).
- [40] S. Karatzikos, A. V. Afanasjev, G. A. Lalazissis, and P. Ring, *Phys. Lett. B* **689**, 72 (2010).
- [41] Y. Tian, Z. Y. Ma, and P. Ring, *Phys. Lett. B* **676**, 44 (2009).
- [42] J. F. Berger, M. Girod, and D. Gogny, *Comput. Phys. Commun.* **63**, 365 (1991).
- [43] J. Dobaczewski, A. V. Afanasjev, M. Bender, L. M. Robledo, and Y. Shi, *Nucl. Phys. A* **944**, 388 (2015).
- [44] M. Bender, P.-H. Heenen, and P.-G. Reinhard, *Rev. Mod. Phys.* **75**, 121 (2003).
- [45] J. Boguta and R. Bodmer, *Nucl. Phys. A* **292**, 413 (1977).
- [46] S. Typel and H. H. Wolter, *Nucl. Phys. A* **656**, 331 (1999).
- [47] J. Dobaczewski, W. Nazarewicz, and P.-G. Reinhard, *J. Phys. G* **41**, 074001 (2014).
- [48] P. G. Reinhard and W. Nazarewicz, *Phys. Rev. C* **81**, 051303(R) (2010).
- [49] A. V. Afanasjev, S. E. Agbemava, D. Ray, and P. Ring, *Phys. Rev. C* **91**, 014324 (2015).
- [50] J. Erler, K. Langanke, H. P. Loens, G. Martinez-Pinedo, and P.-G. Reinhard, *Phys. Rev. C* **85**, 025802 (2012).
- [51] M. Bender, W. Nazarewicz, and P.-G. Reinhard, *Phys. Lett. B* **515**, 42 (2001).
- [52] A. Sobczewski and K. Pomorski, *Prog. Part. Nucl. Phys.* **58**, 292 (2007).
- [53] A. Pastore, J. Margueron, P. Schuck, and X. Viñas, *Phys. Rev. C* **88**, 034314 (2013).